Magnetically Maneuvered Bioceramic Nanostructures Cures Dental Hypersensitivity

Shanmukh Peddi [1,4], Prajwal Hegde [1,4], Prannay Reddy [2], Anaxee Barman [1], Arnab Barik [2], Debayan Dasgupta [1,4] *, Ambarish Ghosh [1,3,4] *

[1] Centre for Nano Science and Engineering, Indian Institute of Science, Bangalore 560012, India

[2] Centre for Neuroscience, Indian Institute of Science, Bangalore 560012, India

[3] Department of Physics, Indian Institute of Science, Bangalore 560012, India

[4] Theranautilus Private Limited, Bangalore 560012, India

*Corresponding authors

Keywords: *Magnetic Nanomedicine, dental hypersensitivity, active matter, bioactive glass*

Abstract

Dental hypersensitivity is an acute pain triggered by everyday stimuli, like extremes of temperature or pH, affecting more than one billion people worldwide. The condition occurs when dentinal tubules are exposed through enamel loss or cementum erosion of the tooth, stimulating nerves located in the peripheral odontoblast zone of the pulp. Existing treatments, such as sensitive toothpastes and adhesive resins, offer short-term relief and are often ineffective, leaving patients reliant on continuous interventions. Here, we demonstrate a new approach to cure dental hypersensitivity using nanoparticles made of magnetic bioactive glass called "CalBots." These sub-micron particles can be maneuvered up to 300 μm deep inside the dentinal tubules for both human and murine teeth, thereafter, triggering the formation of a biocompatible seal and thus preventing response of the exposed tubules and their nerve fibers to external stimuli. We demonstrate CalBots to be non-toxic to animals, at least up to a dosage of 550 mg/kg bodyweight of the animal. Our controlled animal trial experiments, featuring various control groups, demonstrated a remarkable 100% recovery from dental hypersensitivity within the treatment group. In contrast, none of the other groups, encompassing four control groups and one negative control group, exhibited any signs of recovery. The temporal efficacy of our CalBot-based treatment protocol surpasses that of current toothpaste-based solutions available in the market by providing pain relief for a duration orders of magnitude more than the standard 24-48 hours.

Introduction

Dentinal hypersensitivity (DH) is a condition that results in sharp pain triggered by routine activities or common substances encountered in daily life, such as tooth brushing, exposure to cold, sugary, or acidic beverages, or cold air. DH often occurs due to the exposure of dentinal tubules caused by factors like enamel loss or gingival recession[1]. DH [2] is believed to be caused by fluid movement within exposed dentinal tubules due to various stimuli, such as temperature changes, mechanical actions, evaporation, and osmotic forces, as presented in Figure 1(a). This fluid flow within the dentin stimulates nerve endings along the pulp canal, resulting in the sensation of pain, which can range from mild discomfort to severe agony.[3] DH is a globally prevalent issue, affecting the quality of life more than one billion humans.[4–9]

The most popular solution for DH involves blocking the exposed dentinal tubules and isolating the dentinal fluids from the external environment.[10] LASER-induced occlusion of exposed dentinal tubules is also employed for DH. However, it is reported ineffective[11] as it potentially denatures superficial dentine through melting and charring, further compromising dentin microstructure. Desensitizing toothpaste and resin sealing agents provide superficial tubule blockage averaging at 15 μm[12], typically requiring 2-4 weeks for noticeable effects[13]; their efficacy wanes without daily application.[14] Resin-based dentin sealers exhibit less than 10% effectiveness, with no sealing effect after 4 weeks[15], highlighting the need for more enduring DH solutions.

The long-standing technical challenge, therefore, is to achieve a more permanent sealing of the exposed tubules to avoid dislodgement due to local perturbations. One way to solve this challenge is to achieve deeper penetration of the sealant to shield them from local perturbations. In this respect, magnetically guided sub-micron structures provide a promising platform, which has been used previously[16] to achieve greater penetration depths into the dentinal tubule space. Here, we demonstrate a new class of magnetic bioactive glass, referred to as "CalBots," which can reach almost 300μm inside dentinal tubules (see Figure 1 (e),

Supplementary Section S1). Magnetic delivery of CalBots is followed by a controlled self-setting hydraulic cement reaction, wherein they transform into a cohesive matrix of calcium silicate hydrate gel, which undergoes solidification to yield a robust and enduring sealing plug impervious to external influences.

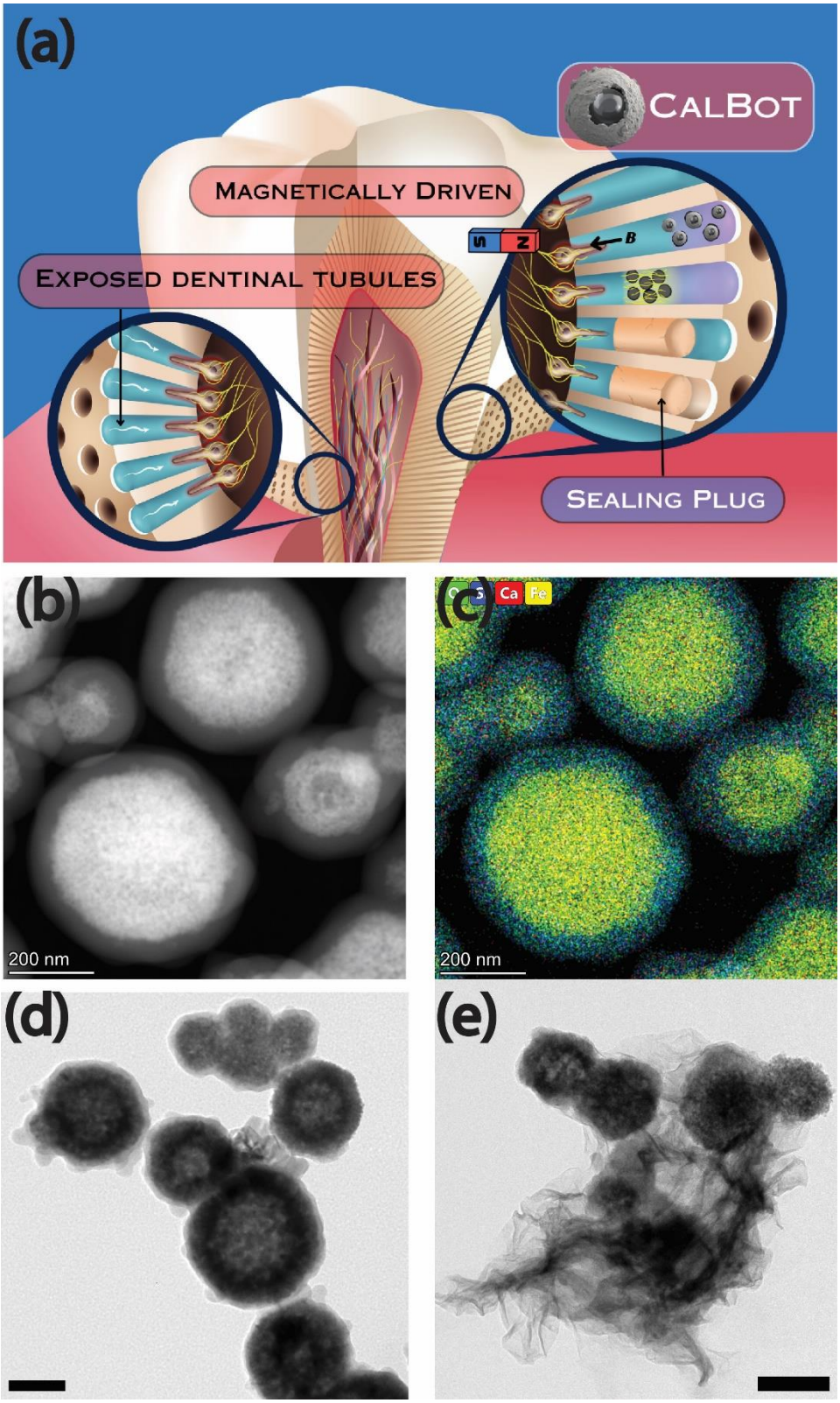

Figure 1 (a) Schematic representation of dental hypersensitivity and the physiology of plug formation inside dentinal tubules using CalBots suspended in CaO solution. (b) High-Angle Annular Dark-Field (HAADF) image of CalBots. (c) Energy Dispersive X-Ray Spectroscopy (EDS) Data of CalBots. Oxygen is colored green, Silicon-blue, Calcium-red, and iron is colored yellow. (d) Transmission Electron Microscope (TEM) image of CalBots suspended in distilled water solution for 30 days presenting absence of any cohesive matrix amongst neighbouring CalBots (e) TEM image of CalBots suspended in CaO solution showing calcium silicate hydrate gel matrix formation. All scale bars represent 200 nm.

Results and discussion

Nanomaterial platform

CalBots, as shown in Figure 1 (b), are approximately spherical core-shell, superparamagnetic structures with an average diameter of 387 ± 55 nm. Nanofabrication details of CalBots are presented in Section 1: Materials and Methods. Further characterization details are given in Section 2: Materials and Methods. The inner core is made of iron oxide enclosed by an outer layer composed of calcium silicate embedded in a silica shell, as shown in the TEM analysis of the CalBots in Figure 1(c). During our therapy, CalBots were suspended in a solution of 1mg/ml calcium oxide (CaO) and water, leading to the formation of calcium hydroxide ($Ca(OH)_2$). The CalBot suspension, in the presence of ambient CO_2, transforms into a cohesive matrix of calcium silicate hydrate gel, which undergoes solidification over 2 – 20 hours to yield a structural matrix imperative for sealing the exposed dentinal tubules.[17,18] This was confirmed by suspending 1mg of CalBots in 1 ml solution of 1mg/ml w/v calcium oxide and a control sample containing CalBots suspended in distilled water. Both the samples were preserved for different time points under sterile conditions, following which TEM imaging (see Figure 1(d) and (e) for comparison) was performed to confirm the formation of a calcium silicate hydrate gel matrix in the CalBot – CaO sample, in contrast to its absence in the control sample for CalBot-DI water.

Interestingly, while medical professionals routinely use calcium silicate-based cement due to their high biocompatibility and osteoconductivity[19], for example, in applications such as orthopedic spinal fusion surgeries,[20] and regenerative dentistry[2122], as far as we know, this safe, biocompatible[22] material platform has never been integrated with magnetic manipulation, and for applications focused on targeting and sealing individual dentinal tubules.

Magnetic manipulation of CalBots for sealing dentinal tubules (*in vitro*) and role of topography

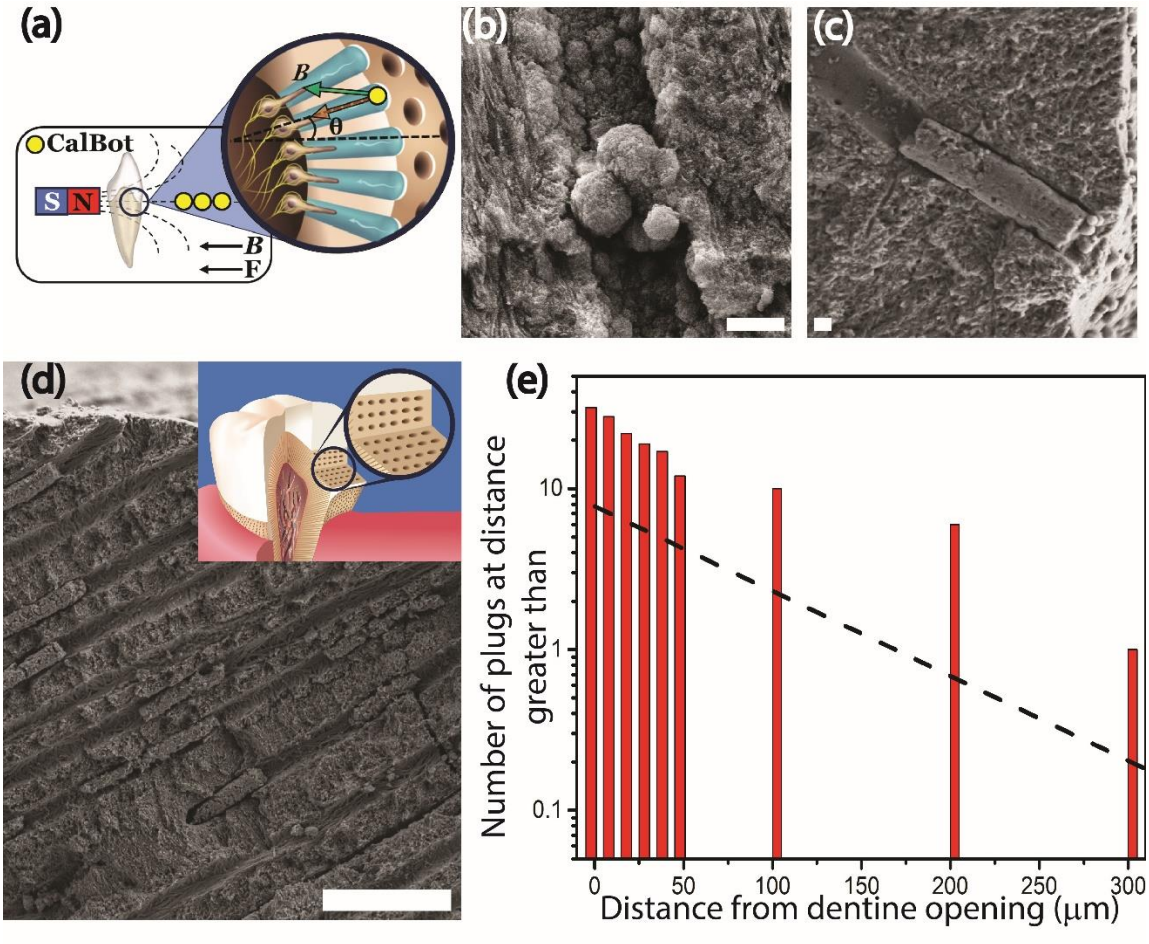

Figure 2 (a) Schematic of CALBOT chains moving towards a permanent magnet inside the tooth. The direction of the magnetic field, B is parallel to the direction of the magnetic force (F). This configuration is ideal for enhancing the penetration of colloidal chains into the dentinal tubules. (b) Scanning Electron Microscope [SEM] analysis of *in vitro* human teeth samples treated with CalBots suspended in distilled water presenting weak plugs formation. (c) SEM analysis of *in vitro* human teeth samples treated with CalBots treatment solution giving structurally robust cementing plugs. (d) Representative SEM image of multiple robust cement plugs formation within the experimentally exposed cross-section of dentine tissue (e) Cumulative count of CalBot plugs observed from the exposed dentine. Most plugs were observed at a depth between 10 to 50μm from the edge of the exposed dentine. The scale bar for (b) and (c) is 500nm. The scale bar for (d) is 10μm.

To demonstrate the penetration of the CalBots deep into the tubules and subsequent plug formation with sealing ability, we performed experiments with *in vitro* human teeth samples (Section 3: Materials and Methods). Figure 2(a) schematic shows that a permanent magnet was used to pull the CalBots deep into the tubules for 10 minutes. Initial experiments with

CalBots suspended in deionized water showed the presence of CalBots up to approximately 300 μm deep inside the dentinal tubule. However, as shown in Figure 2(b), cement plugs or plug-like structures were not formed.

Following this experiment, the CalBots were placed in 1mg/ml w/v solution of calcium oxide-distilled water. Examples of plug formation within a dentinal tubule at similar depths were observed, as shown in Figure 2(c), confirming the importance of CaO in the cementification process.

To gain a quantitative understanding of the penetration of the CalBots under magnetic manipulation, we consider their dynamics under a magnetic gradient field. In agreement with prior work, the CalBots assembled into chains when the field was present. They moved along the direction of the magnetic field lines under the influence of pulling force due to the magnetic gradient field balanced by the hydrodynamic drag. Control experiments performed with CalBots in DI water were used to calculate a single CalBot's velocity and magnetic moment (see Supplementary Section S1 and Supplementary Figure S1). For all results reported in this manuscript, the direction of the magnetic field and its gradient were in the same direction. The speed of the chains was directly proportional to the length of chains, implying larger chain lengths were preferable for greater penetration into the dentinal tubules for a given time of operation. However increasing the magnetic field strength would make it energetically favourable to form bunch formations rather than chains, which will limit their entry inside the tubules. Accordingly, the strength of the magnetic field and density of the particles were carefully chosen in our experiments, as outlined below.

Faraudo et al. [23] reported an aggregation parameter N^* to determine the structure of field-induced self-assembly of superparamagnetic particles into chains. This aggregation parameter is defined as:$N^* = \sqrt{\phi_0 e^{\Gamma-1}}$ where $\phi_0$is the volume fraction of the suspension occupied by CALBOTs, and Γ is a coupling parameter representing the ratio between the maximum value for the attractive magnetic energy and the thermal energy. They are written as: $\phi_0 = \frac{\pi}{6} d^3 n$ and

$\Gamma = \frac{\mu_0 m^2}{2\pi d^3 k_B T}$. In these equations, n is the number of CALBOTs per unit volume, d is the diameter of CALBOTs, m is the magnetic moment, μ_0 is the magnetic permeability of free space, and $k_B T$ is the thermal energy. When $1 < N^* < 10$ the energy balance favours chain formation. Higher N^* causes formations of bundles that may have difficulty entering the dentinal tubule openings. Lower N^* would not favour chain formations, and as a result, adequate plug formations would not be observed. For our experiments, $1 < N^* < 10$ could be maintained with a concentration of $8 \times 10^{19} < n < 8 \times 10^{21}$ for CALBOTs with saturation magnetisation, $m \sim 2.5 - 5 \times 10^{-14} Am^2$. With this n, sufficient length of chain formation was observed and could be manipulated with reasonable velocity.

Topography plays an essential role in cement formation and the chain length possible inside the dentinal tubules. Zaslansky et al.[24] reported that most tubules do not extend at right angles from the dentine-enamel junction. Their orientations change within the first half-millimetre zone beneath the dentin-enamel junction. This change in the orientation of the tubules introduces topography-influenced filtering of longer chain lengths that do not reach greater depths. More cement plugs are formed within the first 100 μm of the exposed dentine, and almost all dentinal openings are closed, as seen in Figure 2(d). However, as depth from the dentine enamel junction increased, fewer plugs were observed. As shown in Figure 2(e), the distribution of the depths beyond which a plug is observed falls exponentially and is extremely rare beyond ~200 μm. This can be explained by the topography of the dentine which prevents longer chains from reaching deeper into the tubules (see Supplementary Figure S1(d) for an example).

Suitability for in vivo applications: animal toxicity studies

The primary rationale for choosing Generally Recognized as Safe (GRAS) materials for CalBots is to prioritize biocompatibility, aligning with our goal to translate research into clinical trials. Before animal trials, we assessed the toxicity of CalBots in twenty female BALB/c mice aged five weeks (see Supplementary Section S2). Grouped according to Table 1 in Supplementary Section

S2, mice underwent intraperitoneal CalBots doses (17.5mg/kg to 550mg/kg) following OECD guideline 425. After a 14-day observation, blood analysis and histopathological examination (see Supplementary Section S3) revealed no mortality or distress signs. Body weight, Total Blood Count (TBC), and serum values aligned with the control group (see Supplementary Section S2, Table 2). Results suggest CalBots, up to 550mg/kg, are safe for mice, indicating potential safety for broader applications.

Efficacy of CalBots in mice

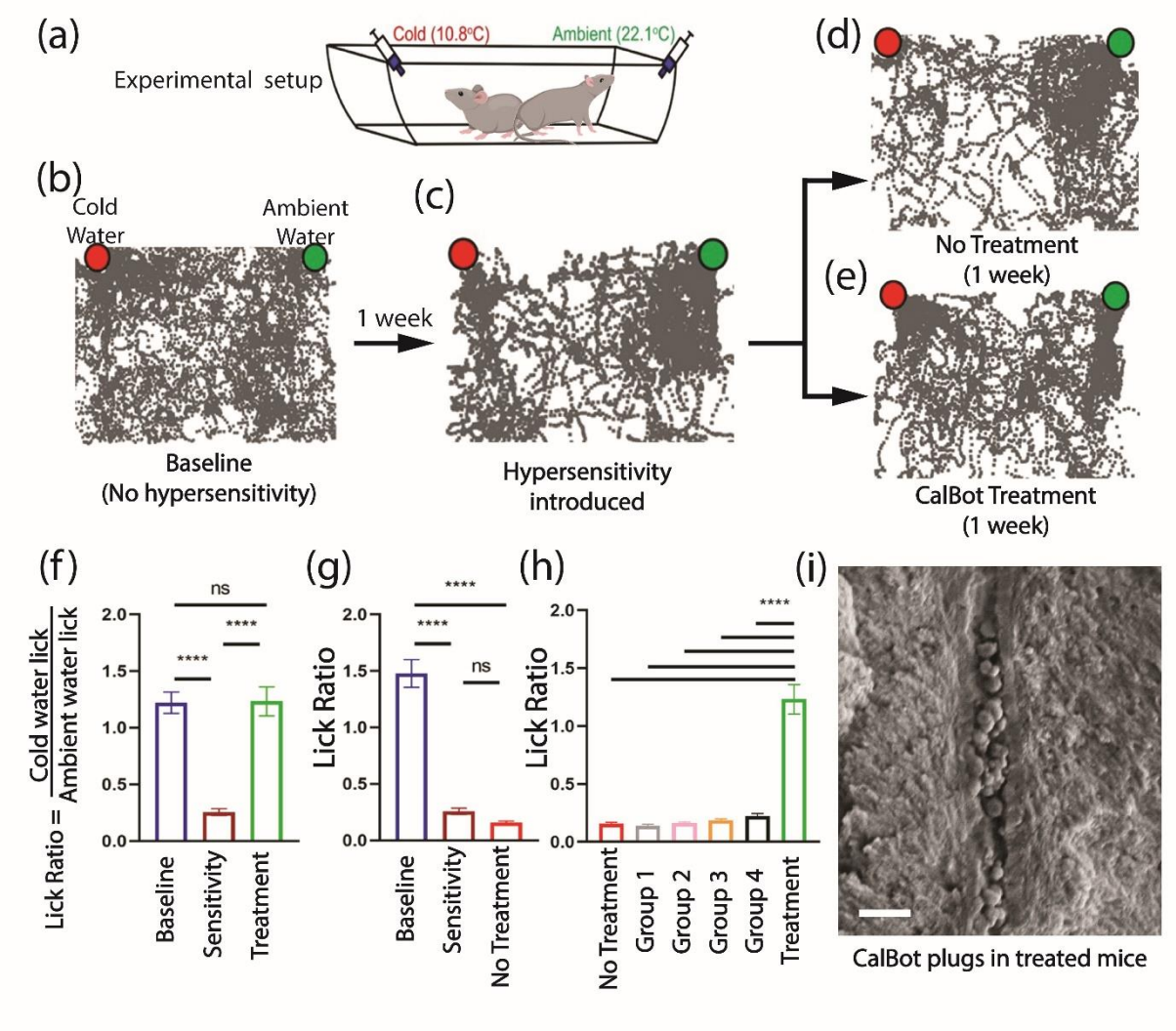

Figure 3:(a) A schematic of the experimental setup used to test the preference (if any) of mice for water of either cold (red spot) or ambient temperature (green spot) during the three phases of the study (Baseline, Sensitivity, and Treatment). The phases last for seven days each in the following order: Baseline phase, induction of sensitivity, Sensitivity phase, administration of treatment/formulation of the treatment/no treatment for control mice, and Treatment/No-Treatment phase. (b) A representative image of the tracking of mice movement using the AI software DeepLabCut during a trial from the first day of the baseline phase, (c)

the sensitivity phase, (d) no treatment administration, and (e) post-treatment administration. Lick ratio: The ratio of the total number of times the mice licked cold water to ambient water during all three phases of the study (42 trials/phase). (f) Mice administered with the treatment where the ratios during baseline, sensitivity, and treatment phases are 1.22, 0.25, and 1.23, respectively, with a one-way ANOVA ****P value < 0.0001 (n=6). (g) Untreated mice where the ratios during baseline, sensitivity, and no treatment phases are 1.47, 0.26, and 0.16, respectively, with a oneway ANOVA, ****P value < 0.0001 (n=6). (h) The ratio of the total number of times the mice licked cold water to ambient water during the treatment phase of the study. The mean Lick Ratio for mice without treatment (n=6), Group 1: treated with calcium oxide solution (n=5), Group 2: treated with iron oxide nanoparticles with a magnet (n=5), Group 3 treated with CalBots (n=5) without magnet), Group4: treated with iron oxide nanoparticles in a calcium oxide solution with a magnet (n=5), and the actual treatment (n=6) was 0.16, 0.14, 0.16, 0.18, 0.22, and 1.23, respectively, with a one-way ANOVA ****P value < 0.0001. (i) *post facto* Scanning Electron Microscope image of treated dentinal tubules in the treatment mice cohort highlighting the formation of cement plug.

Mice teeth are a reliable marker for evoking spontaneous pain, inducing allodynia.[25] We studied the behavioural change in water temperature preference as a proxy for the presence, absence, or treatment of dental hypersensitivity. To assess the efficacy of enamel damage as a model for sensitivity studies, we implemented a preference test (see Section 4: Materials and Methods, Supplementary Section S4, Supplementary Section S5) as illustrated in Figure 3(a) to quantify the preference of healthy mice towards water temperature, which was followed by performing the same preference studies on mice with DH, pre- and post- treatment with CalBots.

Water-deprived mice underwent seven-day baseline trials, ensuring unbiased temperature preferences (see Supplementary Section S4). Dental hypersensitivity (DH) was induced, and a one-day recovery succeeded it. DH trials were conducted for seven days to monitor water temperature preference changes. Post-DH trials, preferences were re-evaluated for both treated and untreated cohorts. In the treatment cohort following the administration of CalBots, there was a period of six hours with no water, followed by water consumption for the remainder of the day. Subsequently, there is a 24-hour no-water consumption period to prepare the mice for experiment day to understand the treatment cohort's preference towards cold or ambient water. Non-treatment mice served as additional controls to check for the longevity of the sensitivity caused. AI-based DeepLabCut© (DLC) software was deployed to avoid human bias, facilitating nose coordinate tracking, and determining water temperature preferences (see Supplementary Movie 1). During baseline trials, mice exhibited no temperature preference as shown in Figure 3(b). Following sensitivity induction, clustering towards ambient-temperature water as shown in Figure 3(c) indicated cold water avoidance, which persisted in untreated mice for a week (see

Figure 3(d)). CalBot-treated mice, however, displayed point clustering near both syringes (see Figure 3(e)), akin to baseline trials, demonstrating reduced cold-water avoidance. Compared to the baseline, the enhanced clustering in treated mice suggests environmental familiarity. Tracking data explicitly affirmed CalBot's efficacy in diminishing cold water aversion without altering baseline preferences.

To understand comparative temperature preference, we introduced a new parameter, i.e., the Lick Ratio, which refers to the comparison of how many times mice licked cold water compared to ambient water in different stages of the study (42 trials for each stage). In the group receiving treatment (Figure 3(f)), the ratios were 1.22 during baseline, 0.25 during sensitivity, indicating strong avoidance towards cold water, and 1.23 during treatment phases, indicating recovery from DH. This showed a statistically significant difference (one-way ANOVA, ****P value < 0.0001, n=6). The ratios for untreated mice (Figure 3(g)) were 1.47 during baseline, 0.26 during sensitivity, and 0.16 during the phase with no treatment, indicating no recovery without treatment intervention. The difference was statistically significant (one-way ANOVA, ****P value < 0.0001, n=6). To evaluate CalBots' efficacy, we conducted experiments with four distinct groups of mice (n=20), each group (n=5) subjected to specific control formulations to replicate sensitivity treatment. After sensitization, all mice (n=20) underwent seven-day sensitivity trials, followed by seven-day treatment trials with assigned formulations.

a. Group 1 (n=5) received a treatment of calcium oxide (CaO) solution to understand the role of CaO as a standalone agent in forming plugs.
b. Group 2 (n=5) received iron oxide nanoparticles (1 mg/ml) in distilled water and were activated using a magnetic array to understand the role of magnetic drive plug formation.
c. Group 3 received a CalBot solution without a magnetic array to understand the efficacy of CalBots without a magnetic drive.
d. Group 4 had iron oxide nanoparticles (1 mg/ml) in a 0.1% w/v calcium oxide solution activated using a magnet array to understand the importance of Calcium silicate in plug formation.

The magnetic array for Groups 2 and 4 matched the one used in phase 1 trials. We plotted the comparative Lick Ratios (Figure 3(h)) for the mice group without treatment, Group 1, Group 2, Group 3, and Group4 of the control groups and the treatment group as 0.16, 0.14, 0.16, 0.18, 0.22 and 1.23 respectively with statistically significant difference (one-way Annova ****P value < 0.0001). We cross-checked the cement plug formation in the dentinal tubules of the treated group of mice by conducting a *post-facto* analysis using a Scanning Electron Microscope on the extracted teeth from euthanized subjects (Figure 3(i)). Amongst the control groups, as evidenced by the Lick Ratios, Group 1 and Group 2 showed no reduction in sensitivity. In Group 3, CalBots and CaO formed temporary superficial plugs, providing one-day relief; however, external factors dislodged them, causing DH relapse. Similar trends in Group 4, attributed to deeper agglomeration of crystalline iron-oxide nanoparticles, occurred due to CaO suspension and magnetic drive on the iron-oxide nanoparticles. Without cementing plug formation, removal of the magnetic field dispersed the crystalline agglomeration, resulting in DH relapse within a day. Trends in Groups 3 and 4 infer how dynamic interplay among CalBots, CaO solution, and the magnetic field plays a cardinal role in better sealing plug formation, thus relieving DH.

Next, we discuss the clinical relevance of our treatment protocol, focusing specifically on the time required for relief. Based on our animal experiments for the treatment cohort, it took a mere 6-hour window for CalBots to form plugs and alleviate DH effectively.

Regarding the longevity of CalBots plugs inside the dentinal tubules, our behavioral observations extended the recovery behavior from DH for at least two weeks post-induction in mice. From a mechanistic standpoint, our findings suggest a plausible duration greater than a month, supported by *post-facto* SEM images displaying CalBot plugs in dentinal tubules of mice teeth (Figure 3(i)) extracted one month after administering the treatment protocol to the mice in the treatment group. In summary, the temporal effectiveness of our proposed CalBot-based treatment protocol stands far superior to contemporary market toothpaste solutions, offering relief for a duration significantly longer than the typical 24-48 hours.

Conclusion

This study presents a novel and effective approach for treating dental hypersensitivity through the strategic blocking of dentinal tubules. Indeed, there have been multiple approaches to using maneuverable nanostructures, also referred to as nanorobots or nanomotors, for therapeutic applications, where the structures were manipulated in human *ex vivo* organs, including human blood[26] and teeth[16], as well under animal *in vivo* conditions such as porcine eyes[27], gastric cavity[28], intraperitoneal cavity[29] and urinary bladder[30] of mice using magnetic fields. These precisely targeted drug delivery approaches are promising yet distinct from our demonstration of targeted regenerative medicine. We present a new application of magnetically maneuvered nanoparticles which can form structural biosimilars to repair and protect the body from degenerative losses and alleviate pain. The ideas and demonstrations in this paper is similar in spirit to Feynman's tiny mechanical surgeons and the dream of "*small machines [which] might be permanently incorporated in the body to assist some inadequately- functioning organ*"[31]

Importantly, our comprehensive toxicity evaluations establish that CalBots exhibit a remarkable level of non-toxicity, emphasizing their safety profile for potential clinical applications. The efficacy of the demonstrated technology convincingly surpasses the current state of the art and establishes the potential of CalBots as a groundbreaking solution for managing DH.

Materials and Methods Section

Section 1: Fabrication of CalBots

The CalBots are fabricated by employing solvothermal synthesis.

Chemical reagents

Iron (III) chloride hexahydrate ($FeCl_3$. $6H_2O$), Sodium citrate dihydrate (Na3C6H5O7. 2H2O), Sodium citrate dihydrate ($Na_3C_6H_5O_7$. $2H_2O$), Anhydrous Sodium acetate (CH_3COONa), Ethylene Glycol ($HOCH_2CH_2OH$), Ammonium Hydroxide (NH_3 H_2O), Tetraethyl orthosilicate ($Si(OC_2H_5)_4$), Calcium nitrate tetrahydrate ($Ca(NO_3)_2$. $4H_2O$), Calcium oxide (CaO) all chemicals are procured from Sigma Aldrich.

Synthesis of Iron oxide nanoparticles

20 mL of Ethylene glycol was taken in a Teflon tube. 0.2 g of Sodium citrate dihydrate was added to the solution, then 1.2 g of sodium citrate acetate. Finally, 1g of Iron chloride hexahydrate was added to the solution. The Teflon tube was placed in the autoclave chamber and kept in the hot air oven at 210 °C for 10-12 hr. After this, the sample was cleaned and suspended in ethanol.

Synthesis of Silica coated Iron oxide nanoparticles.

Iron oxide nanoparticles were suspended in an 85mL ethanol solution.7mL ammonium hydroxide was added, followed by 0.2mL TEOS. The solution was placed under sonication for 90 min. At the end of 90 minutes, the particles were cleaned and suspended in 10 mL ethanol.

Introducing calcium silicate on silica-coated Iron oxide nanoparticles

About 0.2 – 0.4 g of calcium nitrate tetrahydrate was added to a 10 mL silica-coated iron oxide nanoparticles ethanol solution. The particle was magnetically separated from the solution and placed in an oven at 40 °C for drying. The sample is annealed for 2-5 hr at 600 °C in an ambient atmosphere. The final product is called CalBot.

Final formulation

5 mg of calcium oxide was added to 50 mL of DI water. 0.5mg of CalBot was suspended in a 2 mL aliquot of Calcium oxide solution.

Section 2: Characterization of CalBots

We performed comprehensive characterizations of CalBots to establish its physiochemical properties.

Transmission Energy Microscopy (TEM) and Energy Dispersive X-Ray Spectroscopy (EDS) Data Acquisition of CalBots

CalBot powder suspended in Deionized (DI) water was drop-cast on gold coated TEM carbon grid. The sample was dried under an Infrared lamp and desiccated to avoid moisture formation. Titan Themis 300 KV from Thermo Scientific was used to obtain high-resolution TEM images. 300 KV acceleration voltage was used for the analysis. Super-X quad EDS detector was used for elemental analysis. As seen in the TEM image, a core Iron oxide nanoparticle of ~250nm diameter on which Silica and Calcium silicate deposition was performed, bringing the final size to ~350nm. As presented in Figure 4(a), EDS information indicates the presence and composition of four elements, i.e., iron, silicon oxide, and calcium.

X-ray diffraction (XRD) Characterization of CalBots

The CalBot sample was drop cast on Silicon wafer XRD (Rigaku Smartlab) analysis with parallel beam glazing angle configuration by fixing omega value at 3 degrees. This configuration helped us to capture the signal only from the sample, thereby avoiding the signal from the Silicon wafer. Figure 4(b) presents the theta ranges from (10°-80°). Except for the Calcium silicate peak at 32°, all other peaks correspond to Magnetite, which is the chemical configuration of Iron oxide nanoparticles.

Vibrating Sample Magnetometer (VSM) characterization of CalBots

The magnetic moment of the CalBot sample was quantified by employing Vibrating Sample Magnetometer (VSM) characterization on Quantum Design's PPMS Versalab. 1mg of CalBot sample (powder) was filled in an airtight VSM capsule, and the experiment was performed at room temperature, where the applied magnetic field ranges from 30000 Oe to 30000 Oe as presented in Figure 4(c) magnetic moment of the CalBot sample saturated at ~20000 Oe which infers the magnetic properties exhibited by CalBot particles in proximity to a superparamagnetic state.

Fourier Transform Infrared (FTIR) analysis of the CalBots sample.

CalBot powder was mixed with Barium sulfate and turned into a pellet for FTIR scan. The Transmittance is plotted against wave number (Figure 4(d))

Zeta potential and Dynamic Light Scattering (DLS) Characterization of CalBots

Zeta potential and DLS analysis were performed on Zeta PALS (Malvern Panalytical). The surface charge value of CalBot suspended in water is -36.70 ± 4.00 mV, and the particle diameter is 387 (+/-) 55 nm.

X-ray Photoelectron Spectroscopy (XPS) characterization of CalBots

CalBot powder, suspended in Deionized water, was drop-casted onto a copper substrate, and the sample was characterized with XPS (Kratos Axis Ultra). Binding energy range provided for Silicon (95-108 eV), calcium (340-370 eV), Iron (700-740 eV), and Oxygen (520-545 eV). Peak positions were calibrated with respect to adventitious Carbon peak C1s at 284.6. From the XPS data, peaks were observed for Silicon, Calcium, and Oxygen, as represented in Figures 4(e), 4(f), and 4(g), respectively. However, we can observe an absence of peak for Iron (Figure 4(h)). This is because the effective penetration depth of XPS is less than 10nm and in the case of

CalBots, Silica and Calcium silicate act as a barrier. The remaining peaks of Silicon, Oxygen, and Calcium represent the Silica and Calcium silicate compounds.

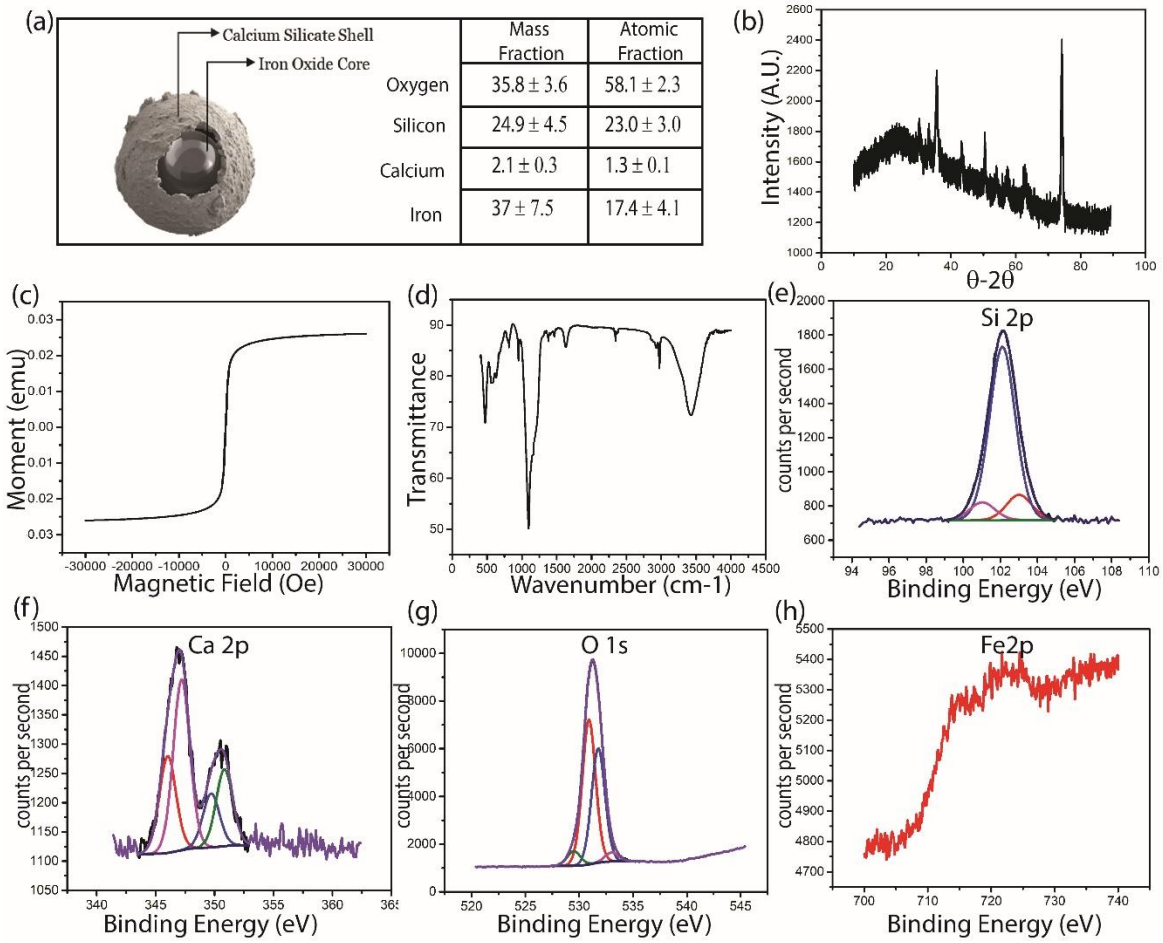

Figure 4(a) Energy Dispersive X-Ray Spectroscopy (EDS) Data Acquisition of CalBots (b) X-Ray Diffraction (XRD) Characterization of CalBots (c) Vibrating Sample Magnetometer (VSM) data analysis of the CalBots. (d) Fourier transform Infrared characterization (FTIR) of CalBots. X-ray Photoelectron Spectroscopy (XPS) characterization of CalBots with peaks observed for (e) Silicon, (f) Calcium, (g) Oxygen, and (h) the peaks were absent for Iron due to the effective penetration depth of XPS is less than 10nm and in case of CalBots Silica and Calcium silicate acts as a barrier.

Section 3: *In Vitro* CalBot cementation experiments

Tooth sample preparation

Human teeth samples were acquired from human subjects, and twenty (n = 20) tooth samples were prepared for performing the *in vitro* experiments. These samples were obtained from Dr. Natasha Valijee and Dr. Prerna Krishna Modi, clinical residents at JSS (Jagadguru Sri

Shivarathreeshwara) Dental College and Hospital, and were cleared by the JSS Dental College Institutional Ethics Committee (Approval Number: JSSDCH26/2020). The sample consisted of freshly extracted maxillary teeth for reasons including orthodontic correction, tooth impaction, and avulsed teeth due to traumatic accidents from age groups ranging from 20 to 55 years free of any cervical and carious lesions. The teeth samples were stored in 0.5% chloramine T-hydrate (Sigma-Aldrich, USA). Enamel defects on the tooth surface were created using a water-cooled low-speed IsoMet-1000 annular saw (Buehler, USA) under a constant speed of 500 rpm. Following the creation of the enamel defects, the tooth was subjected to a cleaning process. The irrigants were used in the following sequence:

1. Ultrapure water (10 ml): Through rinse followed by air drying of the defect area.
2. 17% ethylenediaminetetraacetic acid gel at 6 pH (EDTA; Sigma-Aldrich, USA)
3. Ultrapure water (10 ml) final rinse followed by air drying of the defect area.

Once the tooth samples were primed for the experiment, they were positioned in an artificial jaw to simulate clinical conditions followed by the treatment protocol. In both the groups, the respective CalBots solution was loaded on the defective tooth's surface and was driven using an array of magnets which generated a gradient field of 1500G/cm in along a direction perpendicular to the dentine enamel junction facilitating the drive of CalBots towards the depths of exposed dentinal tubules in contrary to healthy dentinal tubules sealed by a layer of enamel. Teeth in both groups were subjected to treatment for 20 minutes, after which the samples were split along the enamel defect using a chisel and mallet. The samples were then loaded on to the Scanning Electron Microscope (SEM) for analysis of the dentinal tubules corresponding to the enamel defect.

Section 4: Randomized control trials in mice population

Animal trials were conducted in two distinct phases. Phase 1 trials encompassed the evaluation of the treatment protocol's (administration of CalBot suspension in CaO solution) efficacy in

treating a cohort of disease-induced mice population. Phase 2 trials included other control groups, aiming to establish the comparative effectiveness of the treatment protocol. All animal experiments were conducted with strict accordance to protocol approved by the Institutional Ethics Committee (IAEC) of the Indian Institute of Science (clearance from the Institutional ethics committee (CAF/Ethics/991/2023)). In this study, a total of thirty-two (n=32) CD1 mice, comprising an equal number of males and females, aged between 8-12 weeks, and weighing 20-22g, were utilized. For Phase 1 (n=12), of the study, twelve mice were allocated equally into treated and non-treated groups while Phase 2 (n=20) involved twenty mice, equally distributed among four distinct control groups. The assignment of mice to their respective groups was performed randomly. All mice were housed in plastic cages with a controlled temperature of 23^{o}C and a 12-hour light/dark cycle. Commercial pellet diet and autoclaved water were provided *ad libitum* until a day before the experiment at which point the mice were water deprived. All mice underwent a sensitization procedure conducted under anesthesia to artificially induce DH. Following the sensitization protocol the mice were allowed to recover for a day by giving them a pellet diet and autoclaved water *ad libitum*.

Sensitization protocol

Mice were anesthetized with 2% isoflurane/oxygen before and during the surgery. The mice were head fixed in an inverted position on the stereotaxic to allow easy access to the teeth for the experimenter, as illustrated in Figure 5 (a, b) for the ease of visualization of the operating field an operating microscope (3.5X zoom) was also installed. Using a water-cooled handheld drill, the lower mandibular incisors were drilled until the enamel layer was breached and the dull yellow coloured dentin was visibly exposed under the microscope as seen in Figure 5 (c), at which point the drilling was stopped. The mice are allowed to recover for a day by giving them a pellet diet and autoclaved water *ad libitum*.

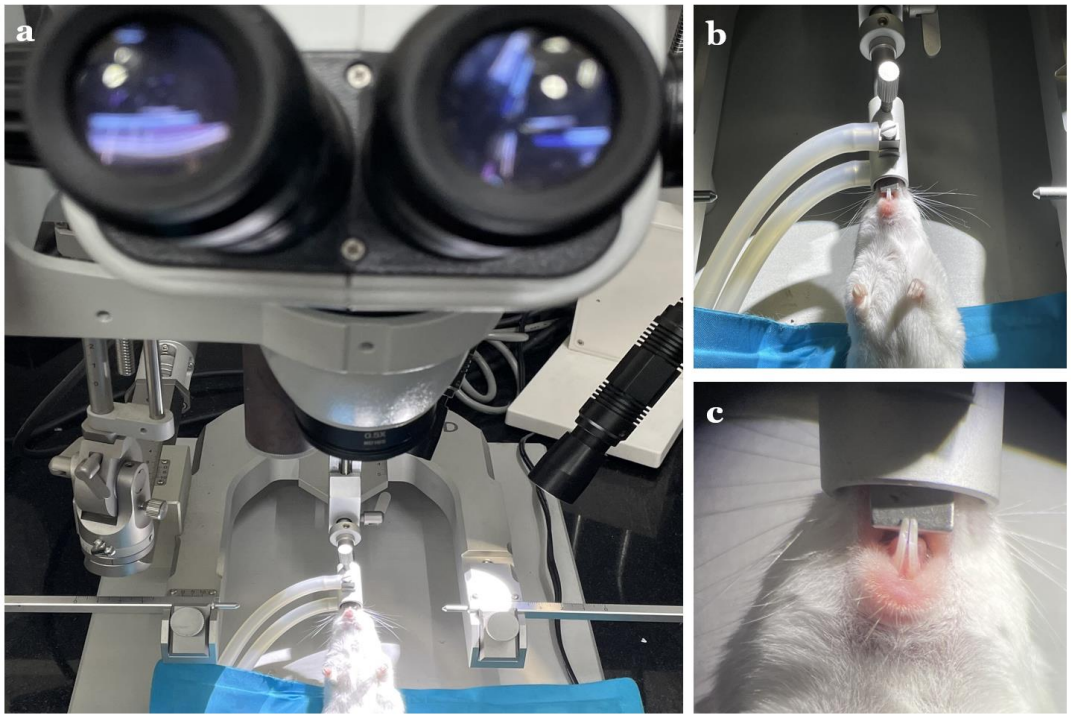

Figure 5 (a, b) Experimental set-up for tooth sensitisation protocol, the mouse's head was fixed in an inverted position on the stereotaxic to allow easy access to the teeth for the operator. (c) 3.5X magnified image of mice incisors.

Behavioural setup and assay

The experimental setup (Figure 3(a)) comprises a plastic enclosure containing two syringes. One syringe is filled with water at ambient temperature, while the other has cold water. To ensure water deprivation, the mice were not provided water for one day before the commencement of the experiment. The mice were placed within the plastic cage, allowing them unrestricted movement to access water from either syringe. Additional water was dispensed upon the mouse licking from a syringe, allowing the mouse to continue drinking from the same syringe or switch to the other. Each trial session was standardized to a duration of 10 minutes. All experimental procedures adhered to the protocols approved by the ethics committee at the Indian Institute of Science.

Treatment protocol for animal trials

Mice were anesthetized using a 2% isoflurane/oxygen mixture before and during the surgical procedure. The mice were securely positioned in a stereotaxic apparatus, with their orientation inverted so that the experimenter had access to their teeth rather than the top of their skulls. In the treatment group of mice (n=6), the treatment procedure involved the application of CalBots to the affected tooth surfaces. 1mg of CalBot powder was uniformly suspended in a 0.1% w/v solution of calcium oxide (CaO) in distilled water, referred to as the CalBot solution. Before applying the CalBot solution, an array of magnets generating a magnetic gradient field of 1500 G/cm was affixed to the lingual side of the incisors in the mice. Subsequently, the CalBot solution was applied to the facial surface of the mandibular incisors, where enamel defects had been induced during the sensitization protocol. The magnet array was left undisturbed on the lingual surface of the incisors for 20 minutes to facilitate the formation of CalBot plugs within the dentinal tubules. In the non-treatment group of mice (n=6), the mice were also positioned in the stereotaxic setup and kept in place for 20 minutes to replicate conditions similar to those of the treatment group without introducing the CalBot solution.

References

1. Gillam, D. G., Aris, A., Bulman, J. S., Newman, H. N. & Ley, F. Dentine hypersensitivity in subjects recruited for clinical trials: clinical evaluation, prevalence and intra-oral distribution. *J Oral Rehabil* **29**, 226–231 (2002).
2. Brännström M. Sensitivity of dentine. *Oral Surgery, Oral Medicine, Oral Pathology* **21**, 517–526 (1966).
3. Rapp R, Avery JK & Strachan DS. The distribution of nerves in human primary teeth. . *Anat Rec* **159**, 89–103 (1967).
4. Rees, J. S., Jin, L. J., Lam, S., Kudanowska, I. & Vowles, R. The prevalence of dentine hypersensitivity in a hospital clinic population in Hong Kong. *J Dent* **31**, 453–461 (2003).
5. Flynn, J., Galloway, R. & Orchardson, R. The incidence of 'hypersensitive' teeth in the West of Scotland. *J Dent* **13**, 230–236 (1985).

6. Fischer, C., Fischer, R. G. & Wennberg, A. Prevalence and distribution of cervical dentine hypersensitivity in a population in Rio de Janeiro, Brazil. *J Dent* **20**, 272–276 (1992).

7. Irwin CR & McCusker P. Prevalence of dentine hypersensitivity in general dental population. *Journal of Irish Dental Association* **43**, 7–9 (1997).

8. Chabanski, M. B., Gillam, D. G., Bulman, J. S. & Newman, H. N. Prevalence of cervical dentine sensitivity in a population of patients referred to a specialist Periodontology Department. *J Clin Periodontol* **23**, 989–992 (1996).

9. Favaro Zeola, L., Soares, P. V. & Cunha-Cruz, J. Prevalence of dentin hypersensitivity: Systematic review and meta-analysis. *J Dent* **81**, 1–6 (2019).

10. Kara, C. & Orbak, R. Comparative Evaluation of Nd:YAG Laser and Fluoride Varnish for the Treatment of Dentinal Hypersensitivity. *J Endod* **35**, 971–974 (2009).

11. Sgolastra, F., Petrucci, A., Gatto, R. & Monaco, A. Effectiveness of Laser in Dentinal Hypersensitivity Treatment: A Systematic Review. *J Endod* **37**, 297–303 (2011).

12. Chen, X. *et al.* Three-dimensional visualization of dentine occlusion based on FIB-SEM tomography. *Sci Rep* **13**, 2270 (2023).

13. Vano, M. *et al.* Reducing dentine hypersensitivity with nano-hydroxyapatite toothpaste: a double-blind randomized controlled trial. *Clin Oral Investig* **22**, 313–320 (2018).

14. Jang, J.-H., Oh, S., Kim, H.-J. & Kim, D.-S. A randomized clinical trial for comparing the efficacy of desensitizing toothpastes on the relief of dentin hypersensitivity. *Sci Rep* **13**, 5271 (2023).

15. Tadano, M. *et al.* The Retention Effect of Resin-Based Desensitizing Agents on Hypersensitivity—A Randomized Controlled Trial. *Materials* **15**, 5172 (2022).

16. Dasgupta, D., Peddi, S., Saini, D. K. & Ghosh, A. Mobile Nanobots for Prevention of Root Canal Treatment Failure. *Adv Healthc Mater* **11**, (2022).

17. Camilleri, J. Hydration mechanisms of mineral trioxide aggregate. *Int Endod J* **40**, 462–470 (2007).

18. Camilleri, J. The chemical composition of mineral trioxide aggregate. *Journal of Conservative Dentistry* **11**, 141 (2008).

19. Liu, Z., He, X., Chen, S. & Yu, H. Advances in the use of calcium silicate-based materials in bone tissue engineering. *Ceram Int* **49**, 19355–19363 (2023).

20. Nagineni, V. V. *et al.* Silicate-Substituted Calcium Phosphate Ceramic Bone Graft Replacement for Spinal Fusion Procedures. *Spine (Phila Pa 1976)* **37**, E1264–E1272 (2012).

21. Prati, C. & Gandolfi, M. G. Calcium silicate bioactive cements: Biological perspectives and clinical applications. *Dental Materials* **31**, 351–370 (2015).

22. Song, W., Sun, W., Chen, L. & Yuan, Z. In vivo Biocompatibility and Bioactivity of Calcium Silicate-Based Bioceramics in Endodontics. *Front Bioeng Biotechnol* **8**, (2020).

23. Faraudo, J., Andreu, J. S., Calero, C. & Camacho, J. Predicting the Self-Assembly of Superparamagnetic Colloids under Magnetic Fields. *Adv Funct Mater* **26**, 3837–3858 (2016).

24. Zaslansky, P., Zabler, S. & Fratzl, P. 3D variations in human crown dentin tubule orientation: A phase-contrast microtomography study. *Dental Materials* **26**, e1–e10 (2010).

25. Rossi, H. L. *et al.* Evoked and spontaneous pain assessment during tooth pulp injury. *Sci Rep* **10**, 2759 (2020).

26. Venugopalan, P. L. *et al.* Conformal Cytocompatible Ferrite Coatings Facilitate the Realization of a Nanovoyager in Human Blood. *Nano Lett* **14**, 1968–1975 (2014).

27. Wu, Z. *et al.* A swarm of slippery micropropellers penetrates the vitreous body of the eye. *Sci Adv* **4**, (2018).

28. Gao, W. *et al.* Artificial Micromotors in the Mouse's Stomach: A Step toward *in Vivo* Use of Synthetic Motors. *ACS Nano* **9**, 117–123 (2015).

29. Yan, X. *et al.* Multifunctional biohybrid magnetite microrobots for imaging-guided therapy. *Sci Robot* **2**, (2017).

30. Vilela, D. *et al.* Drug-Free Enzyme-Based Bactericidal Nanomotors against Pathogenic Bacteria. *ACS Appl Mater Interfaces* **13**, 14964–14973 (2021).

31. Feynman, R. P. There's plenty of room at the bottom [data storage]. *Journal of Microelectromechanical Systems* **1**, 60–66 (1992).